Electronic Supplementary Material (ESI) for ChemComm.
This journal is © The Royal Society of Chemistry 2026

Electronic Supplementary Information (ESI) for

Near-infrared-driven carbon dioxide reduction at 850 nm using water as electron and proton source over a directly connected silver vanadate and zinc rhodate Z-scheme photocatalyst

Jingjing Zhang,[a] Masaomi Yoda,[ab] Masatoshi Yanagida,[c] Toshihiro Takashima,[ab] and Hiroshi Irie*[ab]

[a] *Special Doctoral Program for Green Energy Conversion Science and Technology, Integrated Graduate School of Medicine, Engineering, and Agricultural Sciences, University of Yamanashi, 4-3-11 Takeda, Kofu, Yamanashi 400-8511, Japan*

[b] *Clean Energy Research Center, University of Yamanashi, 4-3-11 Takeda, Kofu, Yamanashi 400-8511, Japan*

[c] *Photovoltaic Materials Group, Center for Green Research on Energy and Environmental Materials, National Institute for Materials Science (NIMS), 1-1 Namiki, Tsukuba, Ibaraki 305-0044, Japan*

Contents

ESI-1) Experimental section

ESI-2) Characterizations

UV–vis spectra of $Ag_2V_4O_{11}$, $ZnRh_2O_4$, and $Ag_2V_4O_{11}/ZnRh_2O_4$ (Fig. S1)

SEM images of $Ag_2V_4O_{11}$, $ZnRh_2O_4$, and $Ag_2V_4O_{11}/ZnRh_2O_4$ (Fig. S2)

ESI-3) CO_2 reduction over $Ag_2V_4O_{11}/ZnRh_2O_4$ under 700 nm LED irradiation (Fig. S3, Table S1)

ESI-1) Experimental

1. Materials

The $Ag_2V_4O_{11}/ZnRh_2O_4$ composite was prepared according to our previous method. Individual catalysts were first synthesized: $Ag_2V_4O_{11}$ was prepared from Ag_2O and V_2O_5 (99.0%, Kanto Kagaku), whereas $ZnRh_2O_4$ was prepared from ZnO (99.0%, Wako) and Rh_2O_3 (99.9%, Kanto Kagaku). Stoichiometric mixtures of these precursors were wet-ball-milled (20 h, ZrO_2 balls) in polyethylene containers and subsequently calcined in air: $Ag_2V_4O_{11}$ at 450 °C for 5 h and $ZnRh_2O_4$ at 1100 °C for 24 h. To form the composite, the two resulting powders were blended at a molar ratio of 0.7:1.7, re-milled under identical conditions, pelletized at 60 kN, and finally calcined again at 450 °C for 5 h to yield the dark brown $Ag_2V_4O_{11}/ZnRh_2O_4$ powder.

2. Characterization

The crystal phases of the $Ag_2V_4O_{11}/ZnRh_2O_4$ composite were analyzed by X-ray diffraction (XRD) using a PW-1700 diffractometer (PANalytical) equipped with a sealed Cu X-ray tube as the radiation source (Cu Kα, λ = 1.5406 Å). Diffuse reflectance UV–visible (UV–vis) spectra were recorded with a spectrometer (V-650, Jasco) over the wavelength range of 300–800 nm, using $BaSO_4$ as the reflectance reference. The photocatalyst morphology was characterized by scanning electron microscopy (SEM; JSM-6500F, JEOL Ltd.).

3. Experiments

Photocatalytic water splitting for H_2 and O_2 evolution was conducted in a gas-closed circulation system. In a typical experiment, 600 mg of the photocatalyst was dispersed in 120 mL of pure water in a large reaction vessel with a cylindrical magnetic stirring bar (40 × 8 mm, AS ONE Corp.). After the vessel was connected to the circulation system, 50 kPa Ar was introduced as the initial atmosphere. The suspension was magnetically stirred during the reaction to ensure a uniform dispersion of the photocatalyst. Irradiation was provided by a monochromatic 850 nm light-emitting diode (LED) at an intensity of 3.2 mW cm^{-2}. The evolved H_2 and O_2 were continuously analyzed using a gas chromatograph (GC-8A, Shimadzu).

Photocatalytic CO_2 reduction was conducted in a similar gas-closed circulation system equipped with a gas chromatograph–mass spectrometer (GCMS-QP 2010 Ultra, Shimadzu), using He as the carrier gas, for product analysis. Three carrier gases, He, H_2, and N_2, are available for use in the GC-MS. When He or H_2 is used as the carrier gas, H_2 cannot be detected, whereas the use of N_2 as the carrier gas prevents the detection of

N_2. Because O_2 evolution is one of the key parameters in this study, the detection of N_2 is important for confirming that air leakage into the reaction system is negligibly small. In addition, the sensitivities for CO and CH_4 detection are lower when N_2 is used as the carrier gas than when He is used. In summary, He was chosen as the carrier gas because it enables the detection of N_2, thereby allowing verification that air leakage into the reaction system is negligibly small, and because it provides higher detection sensitivities for CO and CH_4 than N_2 carrier gas. The mass spectrometer was operated in selective-ion monitoring (SIM) mode, monitoring ions with masses of 16 ($^{12}CH_4$), 17 ($^{13}CH_4$), 28 ($^{12}C^{16}O$), 29 ($^{13}C^{16}O$), and 32 ($^{16}O_2$). The catalyst amount (600 mg), pure water volume (120 mL), and stirring conditions were consistent with those used in the water-splitting experiment. After evacuating the system to remove residual gases, 50 kPa $^{12}CO_2$ was introduced to perform the $^{12}CO_2$ reduction experiments for two cycles. Then, the system was evacuated again, and 50 kPa He was introduced to conduct the control experiment (without CO_2). Isotopic labeling experiments were carried out by introducing 50 kPa $^{13}CO_2$ under the same conditions for two cycles. Each cycle was conducted with the evacuation of the system every 40 h. Irradiation was provided by the same 850 nm LED used in the water-splitting experiments.

ESI-2) Characterizations

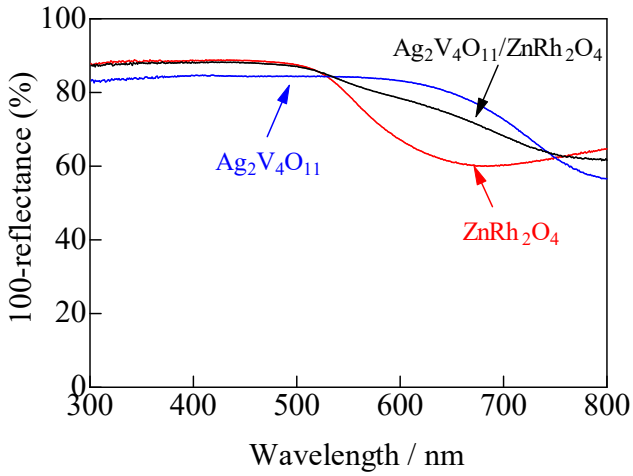

Fig. S1 UV–vis spectra of $Ag_2V_4O_{11}$, $ZnRh_2O_4$, and $Ag_2V_4O_{11}/ZnRh_2O_4$.

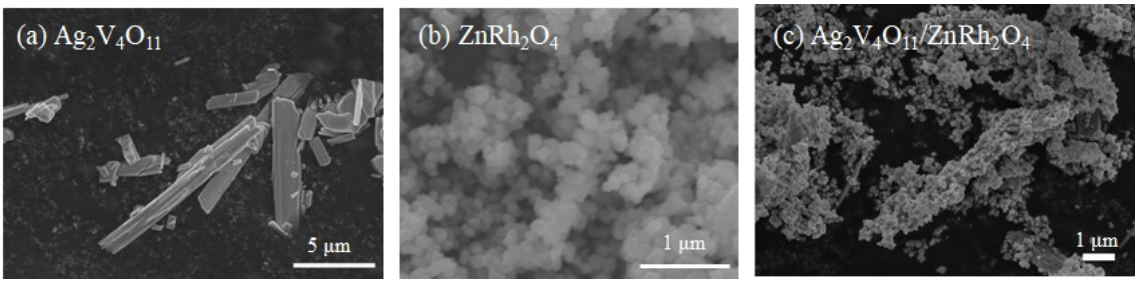

Fig. S2 SEM images of (a) $Ag_2V_4O_{11}$, (b) $ZnRh_2O_4$, and (c) $Ag_2V_4O_{11}/ZnRh_2O_4$. These images are the same as those already published in our previous paper (H. Irie, M. Yoda, H. Miyashita, R. Hanada, T. Takashima, H. Kuroiwa, *Chem. Commun.*, **2023**, *59*, 11057).

ESI-3) CO_2 reduction over $Ag_2V_4O_{11}/ZnRh_2O_4$ under 700 nm LED irradiation (Fig. S3, Table S1)

Using the newly prepared $Ag_2V_4O_{11}/ZnRh_2O_4$ photocatalyst, CO_2 reduction experiments under 700 nm light irradiation were carried out and analyzed by GC-MS. Prior to the CO_2 reduction experiments, He without CO_2 was first introduced under 850 nm light irradiation, and the reproducibility of the newly prepared sample was confirmed from the O_2 evolution rate. The results are shown for the first cycle in Fig. S3. The O_2 evolution rate was calculated to be 0.14 μmol h^{-1}, which was comparable to the value of 0.13 μmol h^{-1} obtained in the third cycle shown in Fig. 3. Similar to the third cycle in Fig. 3, only negligible amounts of ^{12}CO and $^{12}CH_4$ were detected, whereas no ^{13}CO or $^{13}CH_4$ was detected. After evacuating the system, He without CO_2 was again introduced and the sample was irradiated with 700 nm light under the same conditions as those used in the first cycle. The results are shown in the second cycle in Fig. S3. The O_2 evolution rate was calculated to be 0.16 μmol h^{-1}. Because the light intensity at 700 nm (1.1 μW cm^{-2}) was lower than that at 850 nm (3.2 μW cm^{-2}), a direct comparison based on the O_2 evolution rate was inappropriate, and therefore the apparent quantum efficiency (AQE) values were calculated. The AQE for O_2 evolution was 0.064% at 850 nm and 0.24% at 700 nm, indicating that the AQE at 700 nm was 3.8 times larger. In our previous study using a reaction system one-tenth the size of the present experiment (60 mg sample and 12 mL distilled water, ref. 10) H. Irie et al., *Chem Commun*, 2023, **59**, 11057.), the AQE for O_2 evolution was reported to be 0.0015% at 850 nm and 0.0059% at 700 nm, corresponding to a factor of 3.9 increase at 700 nm. Thus, excellent agreement was obtained irrespective of the reaction scale. This result is reasonable because irradiation at 700 nm provides a larger amount of light absorption contributing to the water-splitting reaction. Because the UV–vis absorption spectra shown in Fig. S1 include absorption processes that do not contribute to water splitting, the amount of light absorption involved in the water-splitting reaction cannot be evaluated accurately from these spectra. Although negligible amounts of ^{12}CO were also detected under 700 nm irradiation, no $^{12}CH_4$, ^{13}CO, or $^{13}CH_4$ was detected.

After evacuating the system again, $^{12}CO_2$ was introduced and the sample was irradiated with 700 nm light. The results are shown for the third cycle in Fig. S3. The O_2 evolution rate was calculated to be 0.13 μmol h^{-1}, which was nearly identical to that obtained in the second cycle. Although no ^{13}CO or $^{13}CH_4$ was detected, the amounts of ^{12}CO and $^{12}CH_4$ increased linearly with irradiation time, demonstrating the evolution of ^{12}CO and $^{12}CH_4$. The evolution rates of ^{12}CO and $^{12}CH_4$ were 1.5×10^{-4} and 2.0×10^{-4} μmol h^{-1}, respectively (Table 1). Under 850 nm irradiation, the evolution rate of ^{12}CO was higher than that of

$^{12}CH_4$, whereas under 700 nm irradiation the evolution rate of $^{12}CH_4$ exceeded that of ^{12}CO, showing the opposite tendency to that observed at 850 nm. Although the reason is not clear, further reduction of CO to CH_4 requires that CO remain adsorbed on the photocatalyst surface without desorption. We speculate that CO formation is enhanced under 700 nm irradiation compared with 850 nm irradiation, allowing the reduction to proceed to CH_4 before CO desorption. The wavelength dependence of the CO_2 reduction products will be investigated in more detail in future studies. Because the light intensities differed, the average evolution rates of ^{12}CO and $^{12}CH_4$ obtained in the first and second cycles of Fig. 3 under 850 nm irradiation (3.2×10^{-4} and 1.7×10^{-4} μmol h^{-1}, respectively) cannot be directly compared with those obtained under 700 nm irradiation. Therefore, AQE values were again used for comparison. The AQEs for ^{12}CO evolution at 850 and 700 nm were 3.2×10^{-5} and 2.4×10^{-4}%, respectively, while those for $^{12}CH_4$ evolution were 1.7×10^{-4} and 5.1×10^{-4}%, respectively (Table 1). The AQEs for O_2, CO, and CH_4 evolution were calculated using the equations given below. The AQEs for both ^{12}CO and $^{12}CH_4$ evolution were higher under 700 nm irradiation than under 850 nm irradiation.

The AQEs were calculated using the amount of O_2 evolved and the equation AQE (%) = 100 × 8 × O_2 generation rate/incident photon rate because O_2 generation in the two-step system is an eight-hole process. The AQEs were also calculated using the amount of CO and CH_4 evolved and the equation AQE (%) = 100 × 4 × CO generation rate/incident photon rate and AQE (%) = 100 × 16 × CH_4 generation rate/incident photon rate, respectively, because CO and CH_4 generation in the two-step system is a four- and sixteen-electron process.

The pH of the solution was measured after CO_2 introduction and before light irradiation, as well as after the CO_2 reduction experiment. The pH before irradiation was determined by reproducing the pre-irradiation solution rather than by directly measuring the actual reaction solution immediately before irradiation. Specifically, after dispersing the photocatalyst in pure water and evacuating the system, CO_2 was introduced until the system pressure reached 50 kPa. The solution was then withdrawn from the system, and its pH was measured to be 4.3. The pH after the CO_2 reduction experiment was determined using the actual reaction solution recovered after the CO_2 reduction experiment under 700 nm light irradiation. The pH after the reaction was found to be 5.5. The increase in pH after CO_2 reduction is presumed to result from the consumption of dissolved CO_2 and/or protons in the aqueous solution.

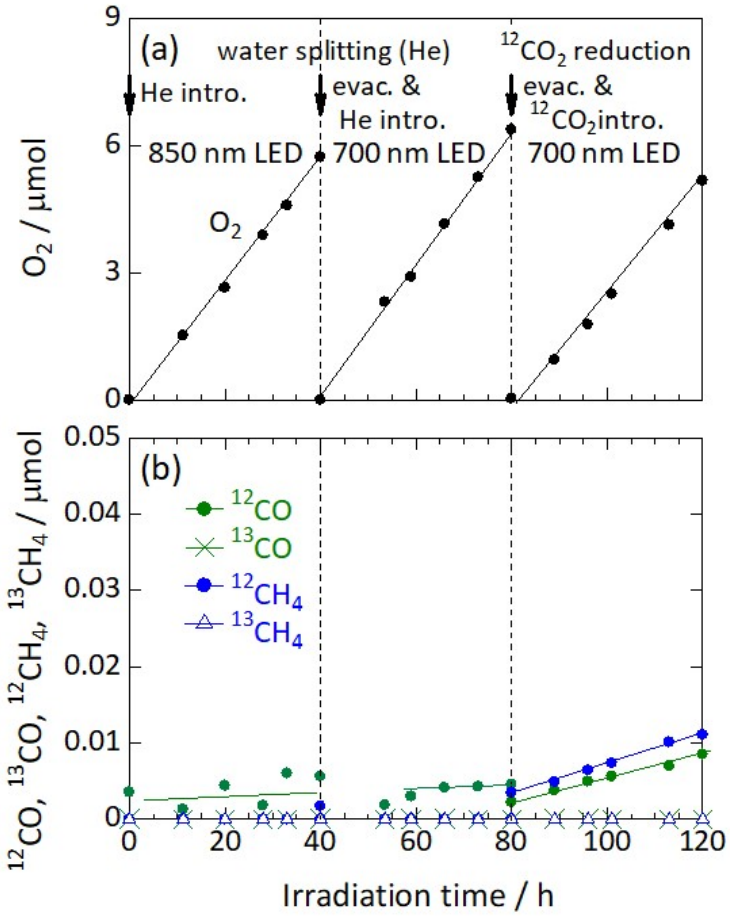

Fig. S3 Time courses of photocatalytic water splitting in the absence of CO_2 (first and second cycles) and CO_2 reduction (third cycle for $^{12}CO_2$ reduction) over $Ag_2V_4O_{11}/ZnRh_2O_4$ under 700-nm and 850-nm LED irradiation at an intensity of 1.1 and 3.2 mW cm^{-2}, respectively. (a) evolution of O_2 and (b) evolutions of ^{12}CO and $^{12}CH_4$ without evolutions of ^{13}CO and $^{13}CH_4$.

Table S1 Generation rates and AQEs of CO and CH_4 under 700 nm and 850 nm light irradiation.

Wavelength / nm	CO generation rate / µmol h^{-1}	CH_4 generation rate / µmol h^{-1}	CO AQE (%)	CH_4 AQE (%)
700	1.5×10^{-4}	2.0×10^{-4}	2.4×10^{-4}	5.1×10^{-4}
850	3.2×10^{-4}	1.7×10^{-4}	3.2×10^{-5}	1.7×10^{-4}